Electronic Supplementary Information

Robust Mn(III) *N*-pyridylporphyrin-based biomimetic catalysts for hydrocarbon oxidations: Heterogenization on non-functionalized silica gel versus chloropropyl-functionalized silica gel

Victor Hugo A. Pinto, Nathália K. S. M. Falcão, Bárbara Mariz-Silva, Maria Gardennia Fonseca, Júlio S. Rebouças*

Department of Chemistry, CCEN, Universidade Federal da Paraíba, João Pessoa, PB, 58051-900, Brazil.

*Author for correspondence: Dr. Júlio Santos Rebouças, Universidade Federal da Paraíba, Departamento de Química, João Pessoa/PB, 58051-900, Brazil, Tel./Fax: +55-83-3216-7591, E-mail address: jsreboucas@quimica.ufpb.br (Júlio S. Rebouças); ORCID: 0000-0003-3818-029X

S1 General Information

4-pyridinecarboxaldehyde (97%, Alfa Aesar), pyrrole (98%, Aldrich), $CHCl_3$ (≥99%, Aldrich), MeCN (99.8%, Carlo Erba), MeOH (99.8%, Vetec), HOAc (99.7%, Dinâmica), (3-chloropropyl)trimethoxysylane (≥97%, Aldrich), n-heptane (Aldrich), and $Mn(OAc)_2{\cdot}4H_2O$ (≥99%, Aldrich) were used as purchased. Silica gel for column chromatography (**SiO_2**, high-purity grade, particle size of 70-230 mesh, median pore diameter 60 Å, Aldrich) was activated as described elsewhere.[1] Toluene (99.5%, Synth) was dried over activated 3 Å molecular sieves (Aldrich).[2] The free-base porphyrins *meso*-tetrakis(2-pyridyl)porphyrin and *meso*-tetrakis(3-pyridyl)porphyrin were purchased from Frontier Scientific Inc. (Logan, UT, EUA). *meso*-Tetrakis(4-pyridyl)porphyrin was prepared as reported elsewhere.[3]

Cyclohexane (Aldrich) was purified for filtration through a SiO_2 plug and stored into amber glass bottle. Adamantane (Fluka) was dissolved in $CHCl_3$ and the resulting solution was filtered through active charcoal and recrystallized. Iodosylbenzene (PhIO) was prepared from (diacetoxyiodo)benzene ($PhI(OAc)_2$, Aldrich) as reported elsewhere.[4] PhIO was stored under refrigeration and its active oxygen content was determined periodically by iodometry.

Elemental analysis (C, H, and N) were carried out on elemental analyzer Perkin Elmer model 2400. Chloride was quantified by Volhard method.

Infrared Spectroscopy (FTIR) spectra were recorded with a Shimadzu IR-Prestige-21 spectrophotometer using KBr pellets in the 400-4000 cm^{-1} range with 32 scans and resolution of 4 cm^{-1}.

UV/VIS spectra were recorded with a Hewlett-Packard 8453 diode-array spectrophotometer or with a Shimadzu UV-1800 spectrophotometer. Diffuse reflectance UV/VIS spectra were recorded with a Varian Cary 100 Bio Spectrophotometer or with a Shimadzu UV-3600 spectrophotometer.

Solid state ^{13}C and ^{29}Si NMR spectra were carried out on Bruker AC300/P spectrometer at room temperature in a 7 mm zirconium oxide rotor. The frequencies used were of 75.47 MHz for carbon and 59.61 MHz for silicon, pulse repetitions of 1 and 3 s, and contact times of 1 and 3 ms, respectively. The Cross-polarization (CP) technique was used with magic angle spinning (MAS) of 10 kHz.

Thermogravimetry and differential thermal analysis (TGA-DTA) were carried out simultaneously with a Shimadzu DTG-60 analyzer, using alumina crucible, under dynamic nitrogen at a flow rate of 50 cm^3 min^{-1} and with a heating rate of 10 ºC min^{-1}.

Specific surface area was measured with a Quantachrome apparatus model nova 2000e at 77 K. Before of the analysis, the samples (~100 mg) were degassed by heating at 150 ºC for 2 h. The specific surface area was determined by using BET method.

Scanning Electron Microscopy (SEM) was recorded with a JEOL JSM 6360-LV microscope using an electronic beam of 15 kV. The samples were metalized with gold.

Transmission Electron Microscopy (TEM) was acquired with a JEOL JEM 1200EX-II microscope using an electronic beam of 100 kV. Sample suspensions in acetone were used to deposit the samples on a carbon film coated copper grid.

Oxidation reactions were analyzed on Shimadzu 14B, Shimadzu 17A, or Agilent 7890B gas chromatographs equipped with flame ionization detector (GC-FID). Hydrogen and synthetic air were used for flame maintenance and nitrogen was used as carrier gas. Alltech Carbowax capillary column (length 30 m, internal diameter 0.32 mm, film thickness 0.25 μm) was used in the Shimadzu 14B and Shimadzu 17A. The Agilent 7890B GC was equipped with an Agilent DB-Wax capillary column (length 30 m, internal diameter 0.32 mm, film thickness 0.15 μm) or an Agilent HP-INNOWax capillary column (length 60 m, internal diameter 0.32 mm, film thickness 0.5 μm). The Alltech Carbowax and Agilent DB-Wax capillary columns were used for analyzing cyclohexane, cyclohexanol, and adamantane oxidation reactions. The Agilent HP-INNOWax capillary column was used for analyzing n-heptane oxidation reactions.

For all substrates (cyclohexane, cyclohexanol, adamantane, and n-heptane) a volume of injection of 1 μL of reaction supernatant was used for gas chromatograph analyses in a split mode (5:1). The flow rates of synthetic air (300 mL min^{-1}) and hydrogen (30 mL min^{-1}) were the same in all analyses.

The temperature method used in the cyclohexane and cyclohexanol substrate systems is shown in Figure S1. The pressure of the carrier gas (nitrogen) used in the capillary column was of 10 psi (flow rate of 0.943 mL min^{-1}). The total time of the chromatographic run was of 5.2 min.

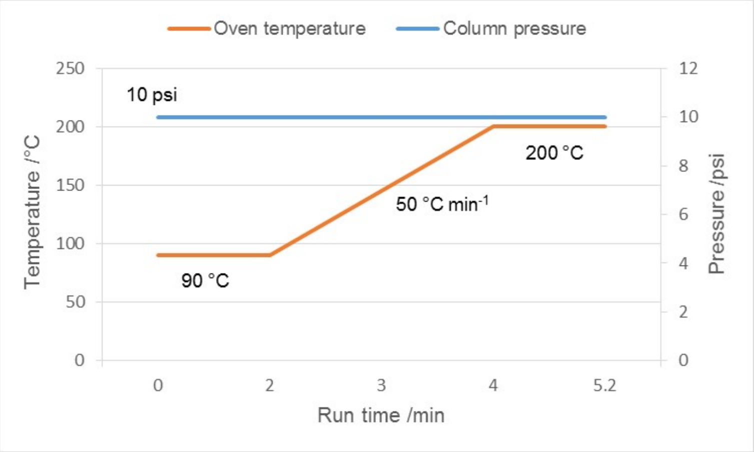

Figure S1. The temperature/pressure method used for analyzing the cyclohexane and cyclohexanol oxidations.

Table S1 exhibits the retention times (RT) for the compounds observed in the chromatograms during analyses of cyclohexane and cyclohexanol oxidations.

Table S1. Retention times (RT) of Cy-one (product), Cy-ol (either substrate or product), bromobenzene (internal standard), and iodobenzene (PhIO reduction coproduct).

Compound	RT /min
Cyclohexanone	2.89
Bromobenzene	3.10
Cyclohexanol	3.38
Iodobenzene	3.86

Figure S2 shows the temperature method used in the adamantane systems. The pressure of the carrier gas (nitrogen) used in the capillary column was of 10 psi (flow rate of 0.900 mL min^{-1}). The total time of the chromatographic run was of 5.6 min. The retention times (RT) of adamantane oxidation products, along bromobenzene (internal standard), and iodobenzene (PhIO reduction coproduct) are summarized in Table S2.

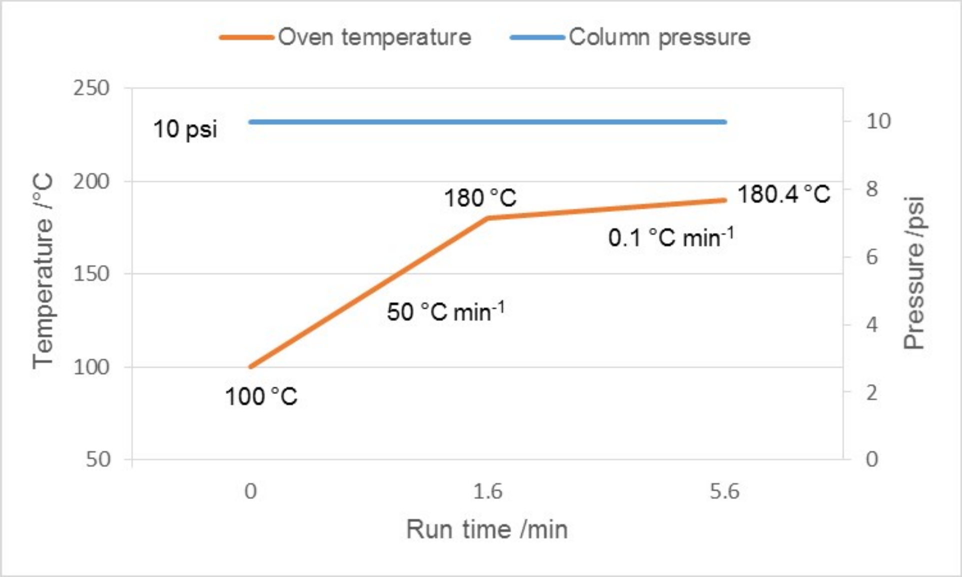

Figure S2. The temperature/pressure method used for analyzing the adamantane oxidations.

Table S2. Retention times (RT) of compounds of relevance to adamantane oxidation analysis: oxidation products 1-adamantanol (Adm-1-ol), 2-adamantanol (Adm-2-ol), 2-adamantanone (Adm-2-one); bromobenzene (internal standard), and iodobenzene (PhIO reduction coproduct).

Compound	RT /min
bromobenzene	2.28
iodobenzene	2.73
1-adamantanol	4.10
2-adamantanone	4.23
2-adamantanol	4.90

For the analyses of n-heptane oxidations, the temperature/pressure method used is shown in Figure S3. The total time of the chromatographic run was of 21.6 min. Table S3 show the retention times (RT) for 10 species observed in the n-heptane oxidation system.

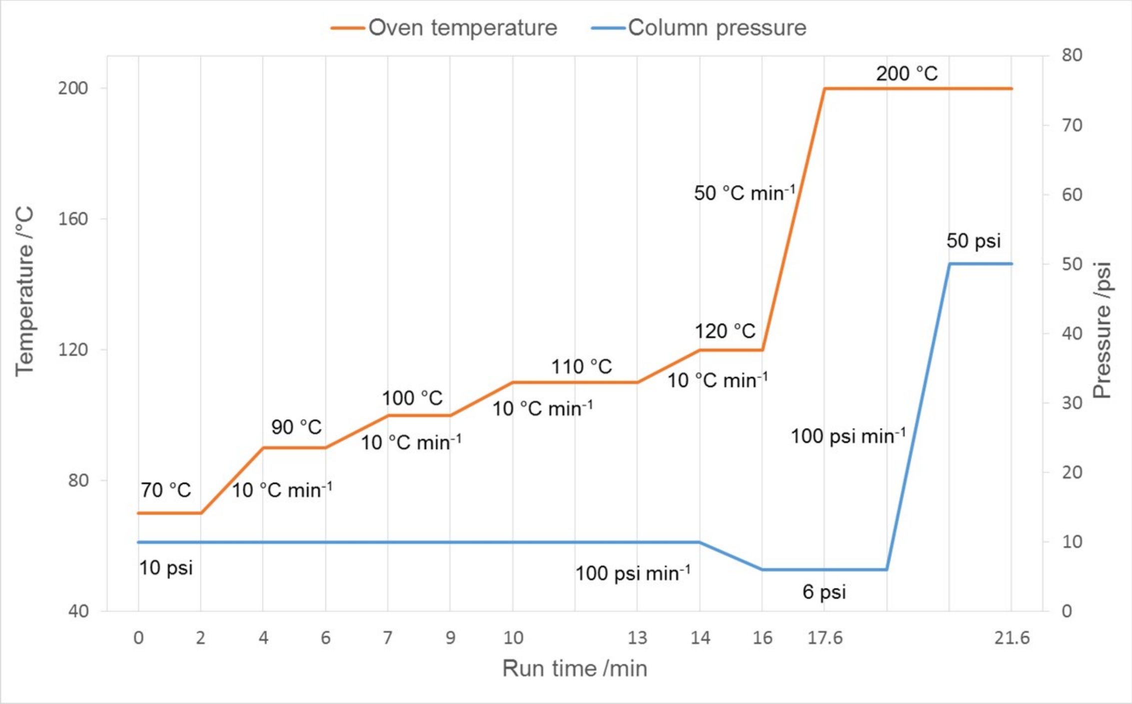

Figure S3. The temperature/pressure method used for analyzing n-heptane oxidations.

Table S3. Retention times (RT) of n-heptane oxidation products, 1-octanol (internal standard), and iodobenzene (PhIO reduction coproduct).

Compound	RT /min
4-heptanone	13.27
3-heptanone	14.11
2-heptanone	15.59
heptanal	15.82
4-heptanol	18.93
3-heptanol	19.04
2-heptanol	19.09
1-heptanol	19.48
1-octanol	19.76
iodobenzene	19.79

S2. Preparation of chloropropyl-functionalized amorphous silica (Sil-Cl)

Sil-Cl was prepared using a slightly modified literature procedure.[5] Briefly, 30.00 g of activated silica gel, 11.9 mL (65.30 mmol) of (3-chloropropyl)trimethoxysilane (CPTS), and 200 mL of dry toluene were refluxed for 72 h, under nitrogen atmosphere. The suspension was filtrated, and the resulting solid was thoroughly washed with toluene, ethanol, and deionized water. The solid was dried in oven at 80 °C for 24 h and stored in tightly capped vials.

S3. Characterizations of SiO_2 and Sil-Cl

FTIR spectra (Figure S4) of unmodified silica gel (**SiO_2**) and **Sil-Cl** showed the vibrations modes at 3450 cm^{-1} (O-H stretching) and at 1630 cm^{-1} (O-H bending) assigned to the silanol groups and physisorbed water molecule.[6-9] The bands assigned to the siloxanes groups appears at 1100 cm^{-1} (Si-O-Si asymmetric stretching), 800 cm^{-1} (Si-O-Si symmetric stretching), and 466 cm^{-1} (Si-O-Si bending). The presence of the carbon chain of chloropropyl moieties is verified by a weak band at 2962 cm^{-1} (C-H stretching) and also by the decreased of the band at 970 cm^{-1} (Si-OH stretching) assigned to the isolated silanol groups.[6-9]

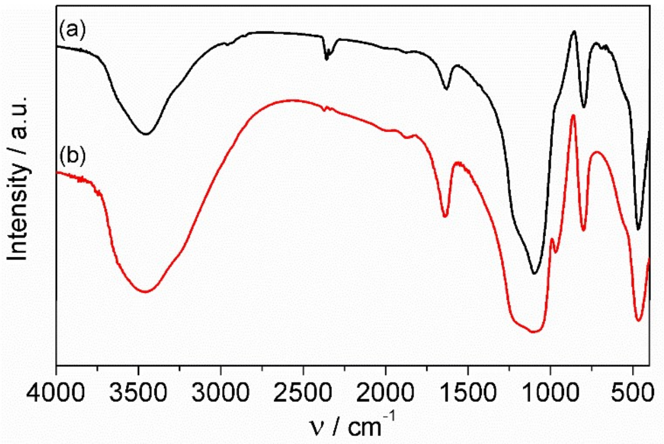

Figure S4. FTIR spectra of (a) **Sil-Cl** and (b) **SiO$_2$**.

In the thermoanalytical curves (TGA-DTA) of **Sil-Cl** (Figure S5) and **SiO$_2$** (Figure S6) were observed two events of weight loss. In the first event in 33-200 ºC temperature range, the weight losses were of 1.9% and 2.4% for **Sil-Cl** and **SiO$_2$**, respectively, which corresponded to physically adsorbed water molecules. The second decomposition event took place from 200 to 900 ºC; for **SiO$_2$**, this event corresponded to a one-step weight loss of 3.1% assigned to the condensation of silanol groups (Si-OH) into siloxanes groups (-Si-O-Si-) and water. From this perceptual loss is possible to determine the amount of silanol groups of **SiO$_2$** (3.4 mmol g^{-1}) and also silanol density (4.9 OH nm^{-2}). These values are consistent with data reported in the literature.[10,11] The second thermal event for **Sil-Cl** took place as multi-step weight loss of 9.4%, which agrees with the presence of the chloropropyl chain in the silica gel surface.[5]

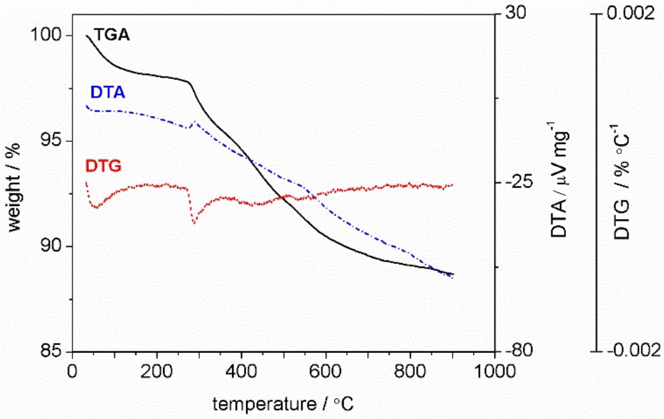

Figure S5. Thermoanalytical curve of **Sil-Cl**.

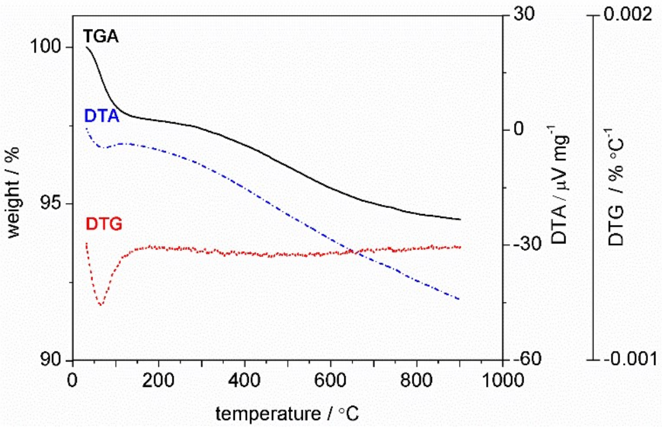

Figure S6. Thermoanalytical curve of **SiO_2**.

The ^{13}C NMR spectrum of **Sil-Cl** (Figure S7) showed strong signals at 11, 28, and 47 ppm assigned to the three methylene carbons ($–CH_2–$) of the chloropropyl chain.[12-14] The absence of a signal at 53 ppm indicates that eventually remaining methoxy groups of immobilized CPTS were completely hydrolyzed to hydroxyl groups upon ethanol and water washings.[12]

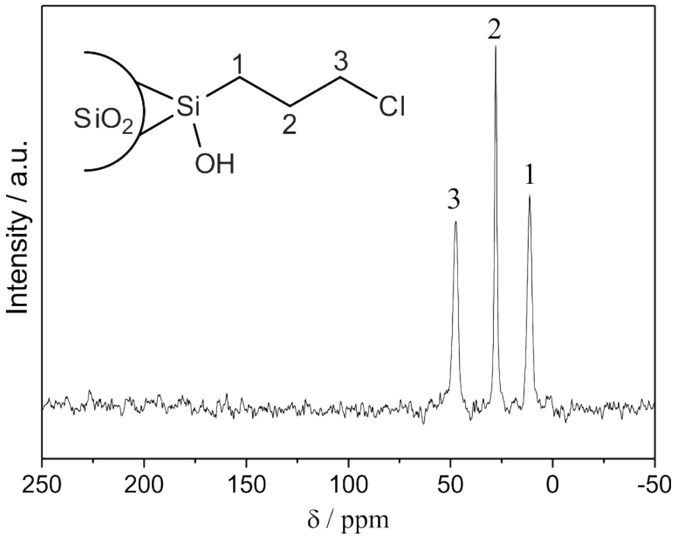

Figure S7. ^{13}C NMR spectrum of **Sil-Cl** and assignments of the signals to the three carbon atoms of chloropropyl moieties.

The ^{29}Si NMR spectrum of **Sil-Cl** (Figure S8) showed chemical shifts assigned to the siloxanes groups (Q^4 species) at –108.9 ppm and at the isolate silanol groups (Q^3 species) at –99.5 ppm.[7,10,12,15,16] The signals associated with the chemical modification of silica surface appeared at –65.7 ppm (assigned to bidentate binding, T^2 species) and –55.4 ppm (assigned to tridentate binding, T^3 species).[7,12,13,16,17] The high intensity of the signals corresponding to T^2 and T^3 species, in addition to the absence of T^1 signal (at about –46 ppm), suggests the predominant formation of cross-linked organosilane bonds.[12,15,17]

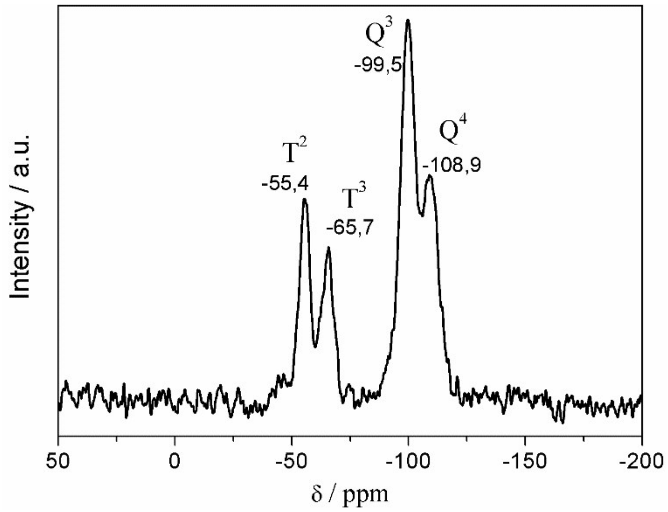

Figure S8. ^{29}Si NMR spectrum of **Sil-Cl**.

The **Sil-Cl** and **SiO_2** specific surface areas were determined by the BET method. The decrease in the specific surface area of **Sil-Cl** (418 m^2 g^{-1}) with respect to **SiO_2** (484 m^2 g^{-1}) occurs as a result of some pores of the silica gel being blocked by chloropropyl moieties, hindering the access of nitrogen gas to these pores during the analysis.[6,18-20]

Figure S9 shows the adsorption-desorption isotherms of **Sil-Cl** at 77 K. The type 4 profile is characteristic of mesoporous materials with the presence of micropores.[9,21,22] Indeed, **Sil-Cl** has a mesopores surface area of 353 m^2 g^{-1} and micropores surface area of 65 m^2 g^{-1}. The H1 hysteresis (Figure S9) indicates that the pores have a form of an open cylinder.[9,21,22] Differently from ordered mesoporous silicas, **Sil-Cl** showed no regular pore size distribution, covering a broad range from 3.6 to 6.8 nm (Figure S10).

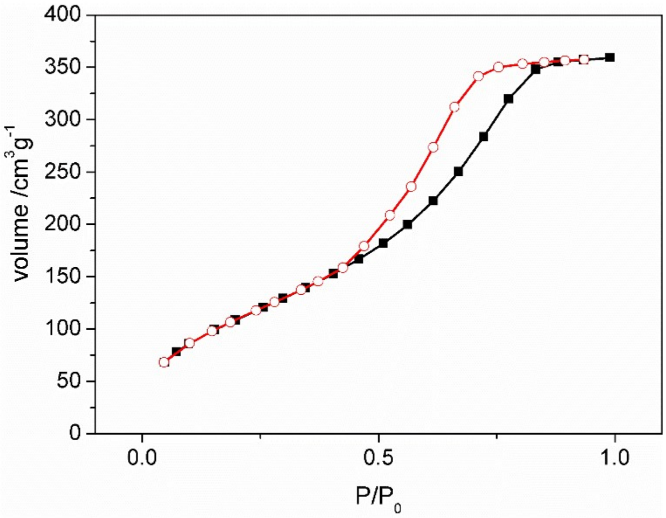

Figure S9. Nitrogen adsorption (full squares) and desorption (empty circles) isotherms of **Sil-Cl**.

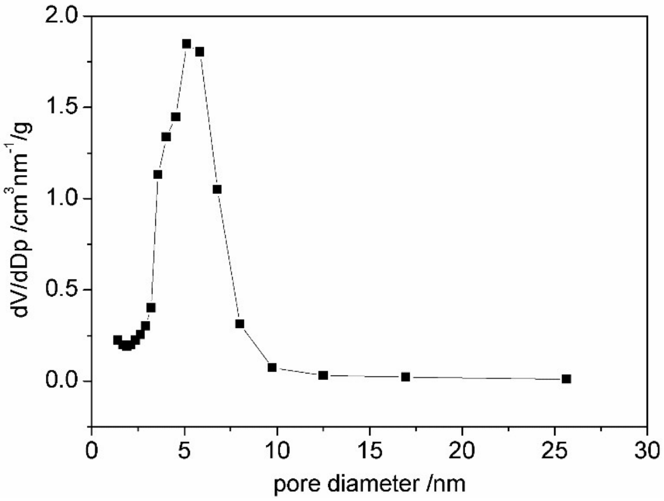

Figure S10. Pore size distribution of **Sil-Cl** by BJH method.

The SEM and TEM micrograph images of **Sil-Cl** shows no apparent differences from those of **SiO$_2$**, indicating that during the functionalization reaction there was no relevant changes in silica gel morphology (Figures S11 and S12). Both solids were characterized by having an amorphous structure with particle sizes in microscale range and the presence of pores.[9,17,20,21]

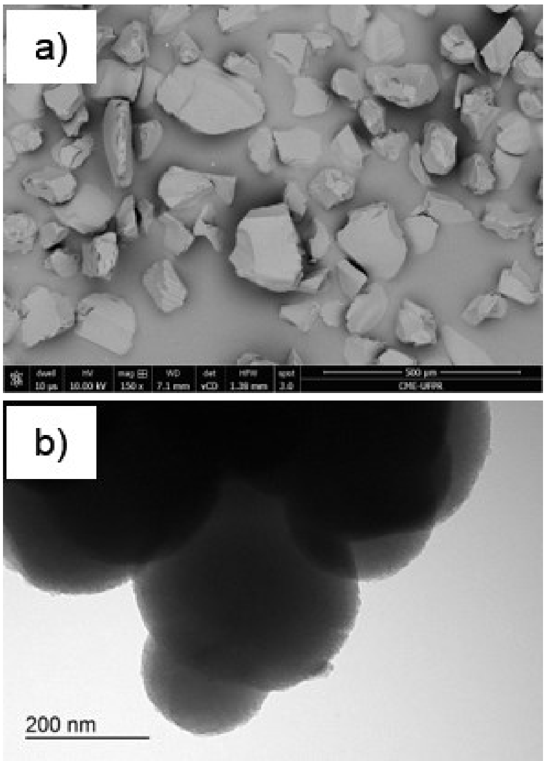

Figure S11. Micrographs of **Sil-Cl** by (a) SEM in the 500 μm scale; and (b) TEM in the 200 nm scale.

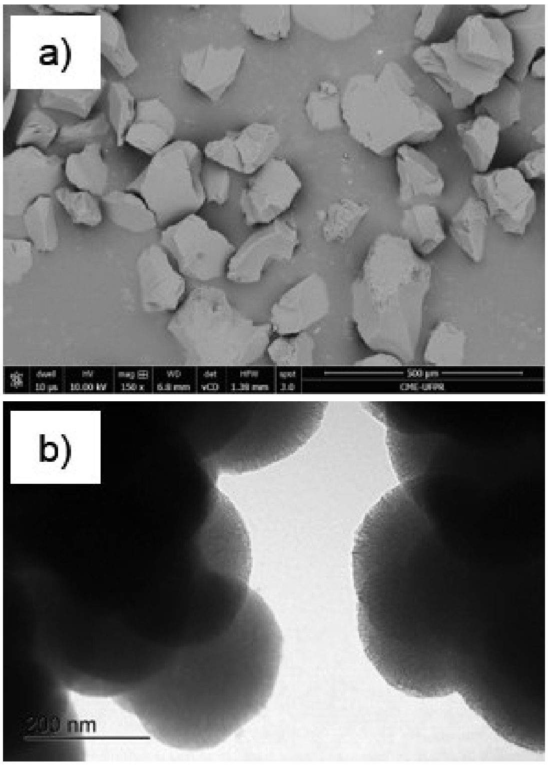

Figure S12. Micrographs of **SiO$_2$** by (a) SEM in the 500 μm scale; and (b) TEM in the 200 nm scale.

S4 Synthesis of Mn(III) *meso*-tetrakis(2-, 3-, or 4-pyridyl)porphyrin chloride, compounds (1), (2), or (3)

Complexes **(1)**, **(2)**, and **(3)** were prepared *via* Mn-metalation of the corresponding free-base porphyrin as reported previously for the *ortho* **(1)** isomer.[1] The isolated complexes were chromatographically and spectroscopically identical to the samples used in our previous study[23]@ and the UV/VIS spectral data of the samples were identical to those reported elsewhere.[1,24,25] UV/VIS spectrum of **(1)** in H_2O λ_{max}/nm (log ε/L mol^{-1} cm^{-1}): 218 (4.67), 285 (4.34), 374 (4.75), 396 (4.70), 462 (5.00), 503 (3.82), 556 (4.10), 633 (3.24), 681 (3.24), 771 (3.34). UV/VIS spectrum of **(1)** in HCl 0.1 mol L^{-1} λ_{max}/nm (log ε/L mol^{-1} cm^{-1}): 254 (4.55), 368 (4.75), 413 (4.42), 456 (5.10), 496 (3.78), 555 (4.09), 781 (3.23). UV/VIS spectrum of **(2)** in H_2O λ_{max}/nm (log ε/L mol^{-1} cm^{-1}): 216 (4.54), 284 (4.21), 376 (4.61), 398 (4.60), 464 (4.88), 510 (3.78), 562 (3.99), 594 (3.80), 684 (3.27), 773 (3.30). UV/VIS spectrum of **(2)** in HCl 0.1 mol L^{-1} λ_{max}/nm (log ε/L mol^{-1} cm^{-1}): 214 (4.62), 256 (4.59), 373 (4.70), 395 (4.67), 460 (5.09), 502 (3.78), 557 (4.08), 678 (3.08), 767 (4.24). UV/VIS spectrum of **(3)** in H_2O λ_{max}/nm (log ε/L mol^{-1} cm^{-1}): 217 (4.55), 376 (4.62), 397 (4.59), 463 (4.87), 506 (3.77), 559 (3.99), 592 (3.71, sh), 680 (3.30), 773 (3.33). UV/VIS spectrum of **(3)** in HCl 0.1 mol L^{-1} λ_{max}/nm (log ε/L mol^{-1} cm^{-1}): 215 (4.67), 236 (4.68), 377 (4.71), 397 (4.70), 461 (5.14), 503 (3.81), 559 (4.13), 677 (3.14), 770 (3.27).

S5 Synthesis of Mn(III) *meso*-tetrakis(*N*-pyridinium-2-, 3-, or 4-il)porphyrin MnPY (Y = 4, 5, 6) in chloride and tosylate forms

MnPY (**Y = 4, 5, 6**) isomers were prepared as chloride salts according to the literature.[26-28] The quality of the samples was evaluated as described for Mn(III) *N*-alkylpyridylporphyins;[23,29] spectroscopic and chromatographic data of isolated **MnPY** (**Y = 4, 5, 6**) samples were identical to those previously reported.[26,29] Tosylate (OTs^-) salts of **MnPY** (**Y = 4, 5, 6**) were also prepared by ion exchange chromatography. Briefly, a methanolic **MnPY** solution (0.92 mmol L^{-1}) was slowly eluted through an ionic-exchange resin (Aldrich, Dowex 2x8, 100-200 mesh) in the tosylate form as reported in the literature;[31] a single fraction was collected and taken to dryness on rotatory evaporator. The Cl^- to OTs^- exchange was characterized by the OTs^- band at 220 nm in the UV/VIS spectrum.[31]

S6 Preparation of Sil-Cl/MnPY (Y = 1, 2, 3) materials

The three **Sil-Cl/MnPY (Y = 1, 2, 3)** materials were prepared by a general procedure as described below for **Sil-Cl/MnP1**.

In a round bottom flask equipped with a mechanical stirrer and a condenser, 19.6 µmol of **(1)** (as a 0.41 mmol L^{-1} aqueous solution) and 5.00 g of **Sil-Cl** were refluxed for 24 h until a full discoloration of the supernatant accompanied by darkening of the solid material was observed. Mechanical stirring was used throughout the immobilization procedure instead of the magnetic stirring, since preliminary attempts with magnetic stirring promoted unwanted grinding of the silica within the magnetic stir bar and the vessel surface, leading to uncontrolled changes in particle size distribution. Upon reaction completion, the suspension was filtered and the solid was washed with small portions of H_2O until the presence of MnP in the washings was not detected by UV/VIS spectroscopy; the washing procedure was repeated with MeOH, EtOH, and finally $CHCl_3$ (in this order). All washings were collected to allow for the spectrophotometric determination of non-immobilized **(1)**. The resulting solid was oven dried at 80 ^{0}C for 24 h to yield 4.86 g of **Sil-Cl/MnP1** as a light orange material. The amount of **(1)** immobilized onto **Sil-Cl** was determined indirectly by UV/VIS spectroscopy by taking the difference between the starting amount of **(1)** and the amount of non-immobilized **(1)** present in the collected washing solutions. MnP loading (in µmol MnP per g of **Sil-Cl**) was calculated as the ratio between the immobilized amount of **(1)** and the starting mass of **Sil-Cl**. The immobilization yield was defined as the ratio between the amounts of immobilized **(1)** and starting **(1)**.

The anchoring of the **(2)** and **(3)** isomers onto **Sil-Cl** followed the same methodology as of **(1)**, except that: (a) for **Sil-Cl/MnP2**, 23.1 µmol of **(2)** (as a 0.48 mmol L^{-1} aqueous solution) and 5.00 g of **Sil-Cl** were used to yield 4.92 g of **Sil-Cl/MnP2** as a light green solid; and (b) for **Sil-Cl/MnP3**, 34.4 µmol of **(3)** (as a 0.72 mmol L^{-1} aqueous solution) and 5.00 g of **Sil-Cl** were used to yield 4.92 g of **Sil-Cl/MnP3** as a light green solid.

These reactions were repeated by an independent coauthor, using independently prepared samples of **(1)**, **(2)**, **(3)**, and **Sil-Cl**, to check for reproducibility. No apparent differences were observed between corresponding **Sil-Cl/MnPY (Y = 1, 2 ,3)** batches.

S7 Preparation of SiO_2/MnPY (Y = 4, 5, 6) materials

The synthesis and workup procedures for the electrostatic heterogenization of the chloride salts of cationic **MnPY** (**Y = 4, 5, 6**) isomers onto **SiO_2** were similar to that described for the **Sil-Cl/MnPY** (**Y = 1, 2, 3**) materials, except that the nature of the starting reagents were changed and the reaction time was shortened to 3 h. For **SiO_2/MnP4**, 18.7 μmol of **MnP4** (as a 0.38 mmol L^{-1} aqueous solution) and 3.59 g of **SiO_2** were reacted to quantitatively yield 3.59 g de **SiO_2/MnP4** as a light orange solid. For **SiO_2/MnP5**, 19.5 μmol of **MnP5** (as a 0.39 mmol L^{-1} aqueous solution) and 4.21 g of **SiO_2** were reacted to quantitatively yield 4.21 g of **SiO_2/MnP5** as a light green solid. For **SiO_2/MnP6**, 18.4 μmol of **MnP6** (as a 0.36 mmol L^{-1} aqueous solution) and 3.69 g of **SiO_2** were reacted to quantitatively yield 3.67 g of **SiO_2/MnP6** as a light green solid. MnPY loadings and immobilization yields were determined as described above for **Sil-Cl/MnPY** (**Y = 1, 2, 3**) materials.

S8 Oxidation reactions

As a general procedure, 2 mL vials were charged with predefined amounts of PhIO, catalyst, 1:1 MeCN:$CHCl_3$ solvent, and substrate (see details below), and sealed with a teflon/silicone septum and a screw cap. The oxidation reactions were carried out at room temperature (*ca.* 26 ºC), under air, in the absence of light, with magnetic stirring. The reactions were quenched at 90 min with 50 μL of a saturated sodium tetraborate and sodium sulfite aqueous solution (the effectiveness of this quenching procedure, as opposed to the use of organic solvents,[32] is presented below, in Section S9). Then, 50 μL of a 28.0 mmol L^{-1} solution of a GC internal standard in MeCN:$CHCl_3$ (1:1, v/v) was added. The products of the reactions were quantified by gas chromatography (GC). Bromobenzene (PhBr) was used as internal standard for the reactions with cyclohexane, cyclohexanol, and adamantane as substrates, while 1-octanol was used in the reactions of n-heptane oxidation. Products were identified by co-elution with authentic standards, which were also used to build the corresponding analytical curves. The reported yields for all products (alcohols, ketones, and aldehyde) represent an average of least three replicates and were calculated based on the initial amount of PhIO (limiting reactant), considering the following stoichiometry: 1 mol of PhIO per mol of alcohol and 2 mols of PhIO per mol of aldehyde or ketones.[1,33,34] For the homogeneous systems (using non-immobilized MnP), MnP destruction (bleaching) was determined spectrophotometrically after quenching with saturated sodium tetraborate and sodium sulfite aqueous solution.

For cyclohexane oxidation (Cy-H), 250 µL of an 1:1 (v/v) MeCN:$CHCl_3$ solvent mixture and 100 µL (0.9 mmol) of Cy-H were added to 0.2 µmol of MnP (**Sil-Cl/MnPY**, **SiO_2/MnPY,** or non-immobilized **MnP**) and either 0.43 mg (2.0 µmol) or 4.30 mg (20.0 µmol) of PhIO, following a MnP/PhIO/Cy-H molar ratio of 1:10:4628 or 1:100:4628, respectively.

For cyclohexanol (Cy-ol) oxidation a MnP/PhIO/Cy-ol molar ratio of 1:10:10 was used to emulate the maximum theoretical Cy-ol produced during Cy-H oxidation. Thus, 100 µL of a 20.0 mmol L^{-1} solution of Cy-ol in MeCN:$CHCl_3$ (1:1, v/v) replaced Cy-H in otherwise identical Cy-H oxidation conditions.

For n-heptane oxidation, 250 µL of a 1:1 (v/v) MeCN:$CHCl_3$ solvent mixture, 150 µL (1.0 mmol) of n-heptane, 0.2 µmol of MnP (**Sil-Cl/MnPY**, **SiO_2/MnPY,** or non-immobilized **MnP**), and 0.43 mg (2.0 µmol) of PhIO were used to yield a MnP/PhIO/n-heptane molar ratio of 1:10:5000.

Adamantane oxidations were investigated at a MnP/PhIO/adamantane molar ratio of 1:10:500, using 750 µL of a 0.14 mol L^{-1} solution of adamantane in MeCN:$CHCl_3$ (1:1, v/v), 0.2 µmol of MnP (**Sil-Cl/MnPY**, **SiO_2/MnPY** or non-immobilized **MnP**), and 0.43 mg (2.0 µmol) of PhIO.

For the recycling studies, the solid catalysts, after the first run, were recovered by centrifugation, washed with $CHCl_3$, EtOH, MeOH, and H_2O (in this order), dried at 80 ºC for 6 h, and, then, reused in a new oxidation run. The reaction media and collected washings were monitored by UV/VIS spectroscopy to verify whether there was leaching of MnPs from the solid catalysts.

The control reactions in the absence of catalysts but containing (i) PhIO+substrate+solvent, (ii) support+substrate+solvent (labeled **Sil-Cl** or **SiO_2** entries), (iii) supports+PhIO+substrate+solvent (labeled **SiO_2**/PhIO or **Sil-Cl**/PhIO entries).

S9. Quenching the catalytic oxidation reactions

Quenching of the oxidations at specific time points was carried out by addition of an aliquot of sodium sulfite/sodium borate inhibitors to the reaction mixture. Although some literature has used the solvent of the catalytic reaction as solvent for these inhibitors as well, we found that the MeCN:$CHCl_3$ (1:1, v/v) mixture was rather ineffective as solvent for the sulfite/borate quenchers. Thus, an investigation of an effective means to quench the oxidation reactions was carried out.

The inhibitor solution was prepared from a mixture of 0.20 g sodium sulfite and 0.20 g sodium tetraborate in 4 mL of the following solvent systems: (a) MeCN:$CHCl_3$ (1:1, v/v), (b) MeOH or (c) H_2O. A couple of cyclohexane oxidation reactions using **(1)** or **Sil-Cl/MnP1** as catalysts were carried out as described in the main experimental section, except that 50 µL of the sulfite/borate quenchers in one of the solvent mixtures was added to the oxidation vial after 1 min of reaction along with the bromobenzene internal standard. Aliquots were periodically analyzed by GC-FID for quantification of the products.

Time course of cyclohexanol production during PhIO-oxidation of cyclohexane catalyzed by **(1)** or **Sil-Cl/MnP1** having sodium sulfite/sodium borate mixtures being added in the reaction vessel after 1 min reaction are presented in Figures S13 and S14. If the quencher is effective, there should be no significant increase in cyclohexanol formation after 1 min. With both catalysts **(1)** or **Sil-Cl/MnP1**, effective quenching was only achieved when water was used as solvent for the inhibitors (Fig. S14, curve c; Fig. S15, curve b).

The inhibitor prepared in the MeCN:$CHCl_3$ (1:1, v/v) mixture was not efficient at all in quenching the oxidation reactions, as sulfite and borate sodium salts were very poorly soluble in this organic solvent mixture (Figure S14, curve a). Indeed, the supposedly “quenched” reaction with sulfite/borate suspended in MeCN:$CHCl_3$ (1:1, v/v) mixture progressed regularly as if not quenched, leading to yields of Cy-ol comparable to those of 90 min uninhibited reactions. The addition of the sulfite/borate mixture as MeOH solution was only able to partially inhibit the oxidation reaction (Figure S14, curve b), due to solubilization of the sodium salts in MeOH. Further investigation was discontinued, and aqueous sulfite/borate solution was used for quenching all oxidation reactions throughout this study.

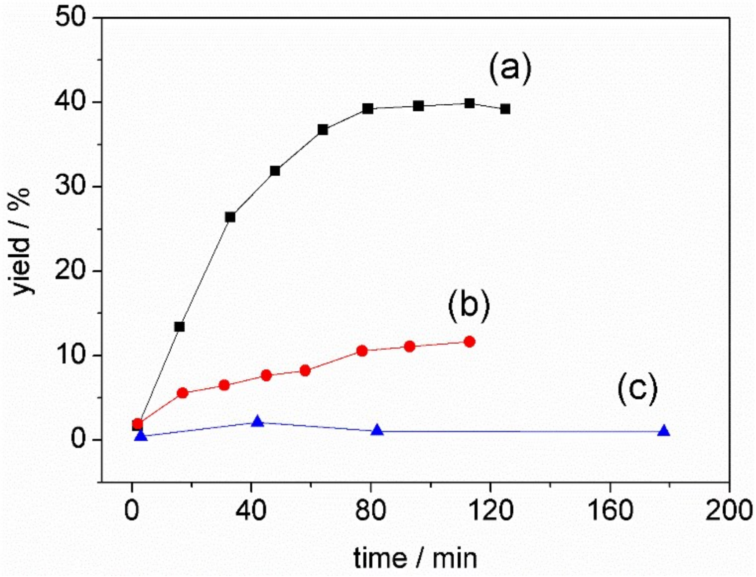

Figure S13. Time course of cyclohexanol production during PhIO-oxidation of cyclohexane catalyzed by **(1)** having sodium sulfite/sodium borate being added in the reaction vessel at 1 min as (a) MeCN:$CHCl_3$ (1:1, v/v) suspension, (b) MeOH solution, and (c) aqueous solution. In aqueous system c, Cy-ol yield was lower than 1% and remained unchanged up to 14 h (data no shown).

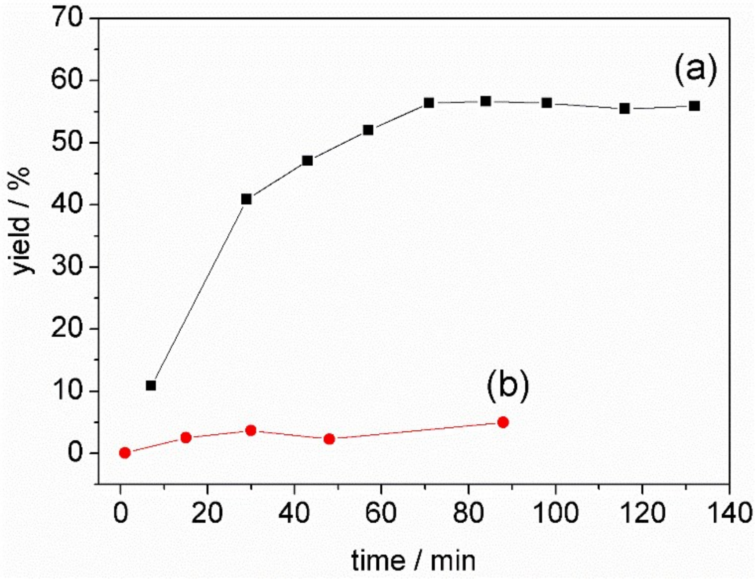

Figure S14. Time course of cyclohexanol production during PhIO-oxidation of cyclohexane catalyzed by **Sil-Cl/MnP1**. Curve (a) reaction without inhibitor; Curve (b) reaction inhibited with aqueous sodium sulfite/sodium borate solution being added after 1 min of reaction.

S10. Cyclohexane oxidations under standard conditions

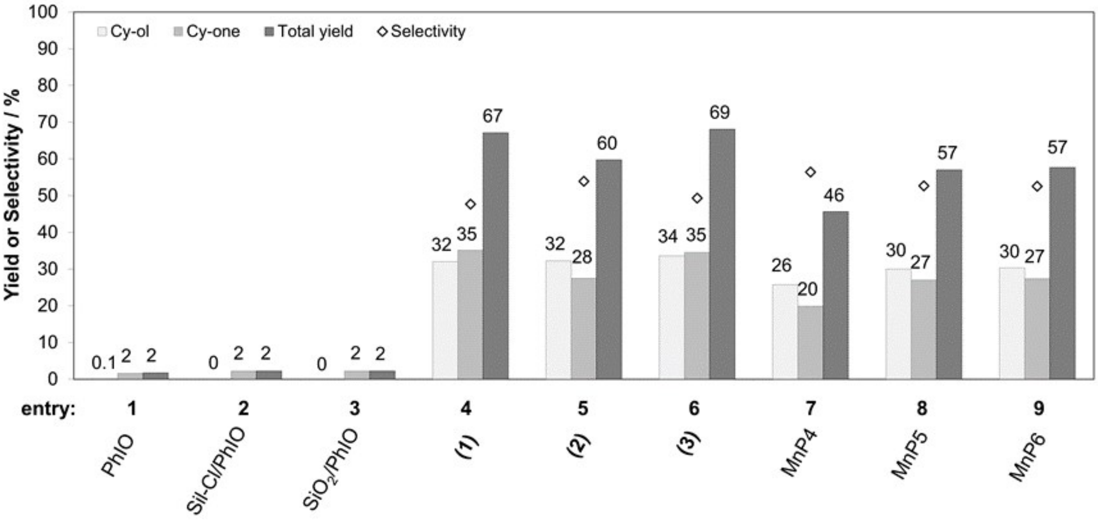

Figure S15. Cyclohexane oxidation reactions by PhIO catalyzed by the non-immobilized MnPs and other controls (only PhIO, Sil-Cl/PhIO, and SiO$_2$/PhIO). Reactions conditions: MnP/PhIO/Cy-H molar ratio of 1:10:4628 (0.2 μmol of MnP, 2.0 μmol of PhIO, 930.0 μmol of Cy-H), MeCN:CHCl$_3$ mixture (1:1, v/v) as solvent, magnetic stirring, 26 ºC, 90 min, and air atmosphere. Yields calculated based on the starting PhIO. 2 mol of PhIO were considered for the formation of 1 mol of Cy-one. Total yield = Cy-ol + Cy-one. Selectivity = 100 x [Cy-ol/(Cy-ol + Cy-one)].

S11. Cyclohexane oxidation under conditions of larger PhIO excess (Cycle A) and reuse under standard conditions (Cycle B)

The oxidative stability of the heterogenized catalysts **Sil-Cl/MnPY** (**Y** = **1**, **2**, **3**) and **SiO$_2$/MnPY** (**Y** = **4**, **5**, **6**) was evaluated using a more drastic condition with a PhIO/MnP molar ratio of 100 in the first reaction cycle (cycle A) followed by the regular reaction condition with a PhIO/MnP molar ratio of 10 in the second reaction cycle (cycle B). The non-immobilized MnP catalysts under homogeneous conditions with PhIO/MnP molar ratio of 100 (cycle A) were also studied for comparison with the corresponding heterogenized systems **Sil-Cl/MnPY** (**Y** = **1**, **2**, **3**) and **SiO$_2$/MnPY** (**Y** = **4**, **5**, **6**). The data of these reactions are presented in Figure S16. The PhIO, **Sil-Cl**/PhIO, and **SiO$_2$**/PhIO control systems (without MnP) showed less than 1% Cy-ol and Cy-one formation.

All catalysts had their catalytic efficiency considerably decreased in the first reaction cycle (Cycle A) with a high PhIO/MnP molar ratio of 100 (Figure S16, entries 1-12) when compared with the corresponding reactions using the regular PhIO/MnP molar ratio of 10 (Figure 5 and 6). This may be related to a series factors,[33,35-37] which include: a) oxidative degradation of immobilized MnPs, since high destruction was observed for the corresponding MnP catalysts under homogeneous conditions (bleaching of about 98% for non-immobilized **(1), (2),** and **(3)** isomers and *ca.* 70% for non-immobilized **MnPY** isomers); b) blocking of access to the MnP catalytic center by large excess of PhIO; c) competing side-reactions such as solvent oxidation;[34,38] d) PhIO disproportionation toward PhI and $PhIO_2$.[39,40] To check whether the use of high oxidant content deactivated and/or destroyed the heterogenized catalysts, the solid materials were recovered and subjected to a new cycle (Cycle B, Figure S17), using a regular PhIO/MnP molar ratio of 10, to which there already are solid data (presented above, Figures 5 and 6), mimicking the conditions of cycles 1, 2, and 3.

For **Sil-Cl/MnP2** and **Sil-Cl/MnP3**, the total yields in cycle B (Figure S17, entries 2 and 3) were much lower than those in cycle 2 (Figure 5, entries 5 and 8), suggesting that both the oxidative degradation of MnP and blocking of MnP by PhIO or its by-product residues may have happened during Cycle A under large excess PhIO. **Sil-Cl/MnP1**, **SiO_2/MnP4**, and **SiO_2/MnP6** seems to have been subjected predominantly to some blocking of PhIO or substrate access to MnP during Cycle A, since the total oxidation yields in Cycle B (Figure S17, entries 1, 4, and 6) are comparable to those in cycle 2 (Figure 5, entry 4 and Figure 6, entries 2 and 8), indicating a recovered catalyst efficiency. **Sil-Cl/MnP1**, **SiO_2/MnP4**, and **SiO_2/MnP6** were not significantly deactivated or oxidatively destroyed by using high PhIO excess during Cycle A and comprise, thus, the most resistant materials against oxidative destruction among the heterogenized catalysts **Sil-Cl/MnPY** (**Y** = **1**, **2**, **3**) and **SiO_2/MnPY** (**Y** = **4**, **5**, **6**).

The catalytic robustness exhibited by **Sil-Cl/MnP1** may be related to the protection exerted on the immobilized MnP by the surface chloropropyl groups of **Sil-Cl**. The excess of about 200 chloropropyl groups per MnP anchored on the surface is likely acting as a shield, preventing bimolecular PhIO-oxidative destruction of the heterogenized MnP. Additionally, a putative parallel orientation of **(1)** in relation to **Sil-Cl** surface may also be contributing to larger oxidative stability. In this situation, MnP would be less exposed to the reaction medium, having one of its sides fully protected by the **Sil-Cl** surface. Another hypothesis to be considered is the influence of steric and electronic factors associated with the binding of the **Sil-Cl** surface alkyl chain to **(1)** *ortho* positions, hampering oxidative attack to vulnerable porphyrin *meso* positions, resembling a recurring porphyrin-based biomimetic feature known as "the *ortho* effect".[4,36,48,58-60] Likewise, the oxidative stability of **SiO_2/MnP4** and **SiO_2/MnP6** materials may be related to the putative parallel orientation of **MnPY** with respect to the **SiO_2** surface; **MnP4** is also subjected to a protective "*ortho* effect".

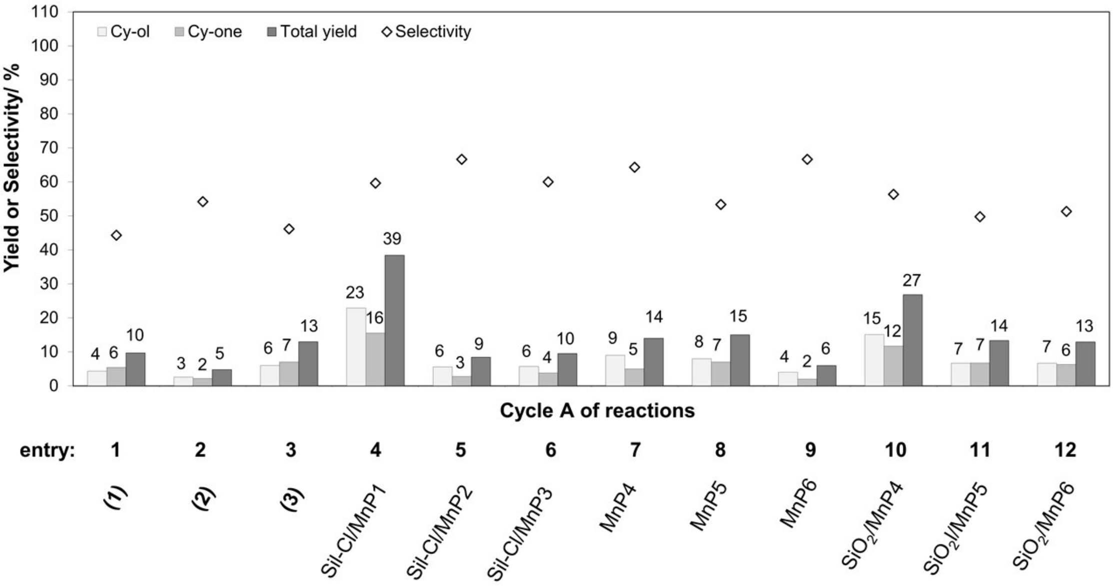

Figure S16. Cycle A of cyclohexane oxidation reactions by PhIO catalyzed by the non-immobilized MnPs and heterogenized materials **Sil-Cl/MnPY** and **SiO_2/MnPY**. Reactions conditions: MnP/PhIO/Cy-H molar ratio of 1:100:4628 (0.2 µmol of MnP, 20.0 µmol of PhIO, 930.0 µmol of Cy-H), MeCN:$CHCl_3$ mixture (1:1, v/v) as solvent, magnetic stirring, 26 ºC, 90 min, and air atmosphere. Yields calculated based on the starting PhIO. 2 mol of PhIO were considered for the formation of 1 mol of Cy-one. Cyclohexane = Cy-H, Cyclohexanol = Cy-ol, cyclohexanone = Cy-one, total yield = Cy-ol + Cy-one. Selectivity = 100 x [Cy-ol/(Cy-ol + Cy-one)].

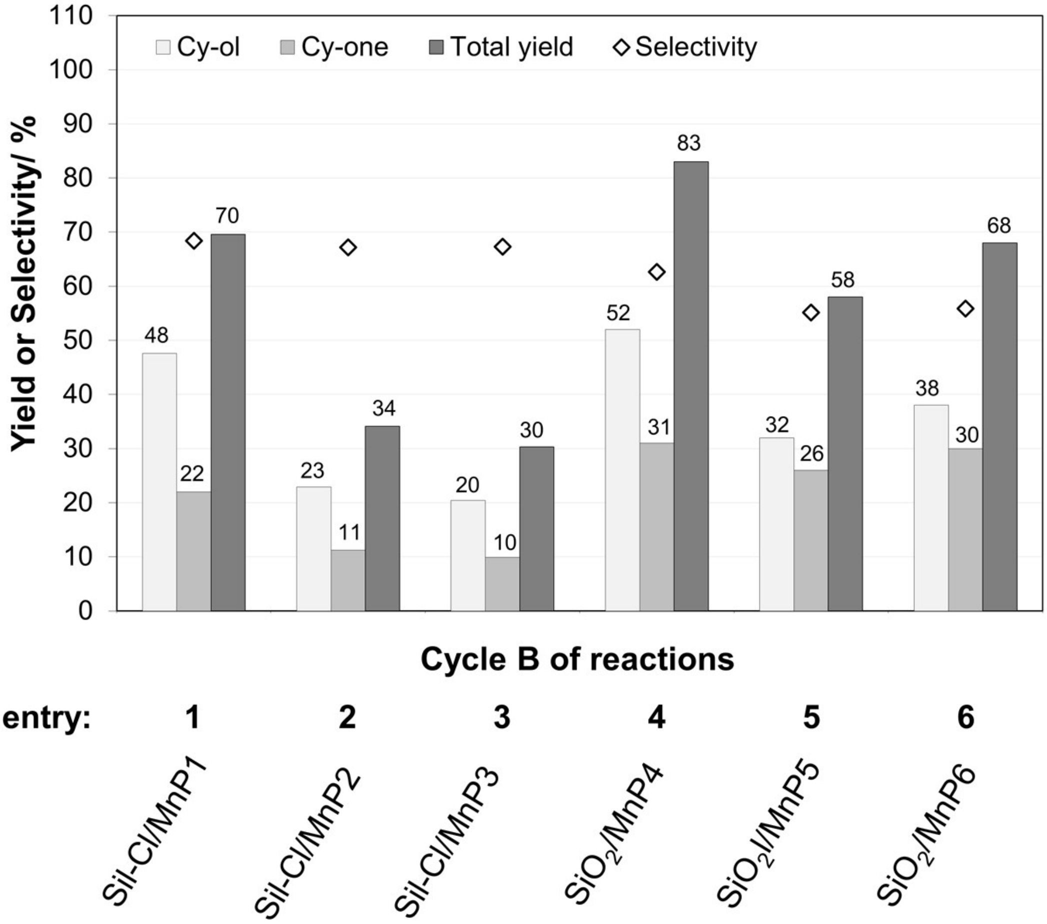

Figure S17. Cycle B of cyclohexane oxidation reactions by PhIO catalyzed by the supported materials **Sil-Cl/MnPY** and **SiO_2/MnPY** after completion of Cycle A (Fig. S18) and catalyst recovery. The reaction conditions were identical to those of Figure S16, except that the MnP/PhIO molar ratio was of 1:10 (0.2 µmol of MnP, 2.0 µmol of PhIO). Yields calculated based on the starting PhIO. 2 mol of PhIO were considered for the formation of 1 mol of Cy-one. Cyclohexane = Cy-H, Cyclohexanol = Cy-ol, cyclohexanone = Cy-one, total yield = Cy-ol + Cy-one. Selectivity = 100 x [Cy- ol/(Cy-ol + Cy-one)].

S12. Oxidation of n-heptane

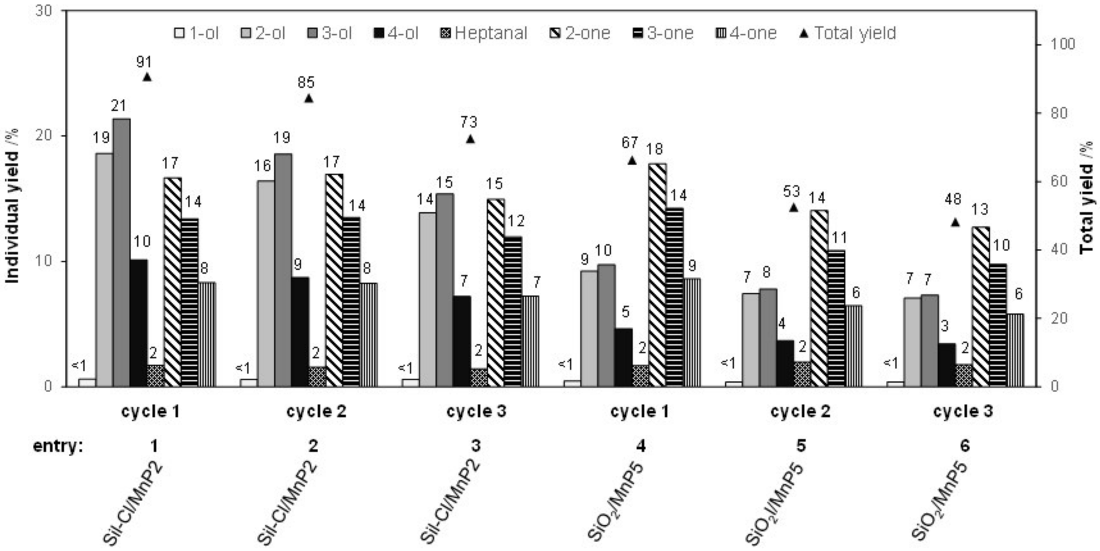

Figure S18. First cycle (cycle 1), second (cycle 2), and third (cycle 3) cycles of n-heptane oxidation reactions by PhIO catalyzed by the supported materials **Sil-Cl/MnP2** and **SiO_2/MnP5**. After completion of cycle 1, the catalysts were recovery and reused for twice more consecutively (cycles 2 and 3). The reaction conditions were identical to those of Figure 5, except that n-heptane replaced cyclohexane and the MnP/PhIO/n-heptane molar ratio was of 1:10:5000. Yields calculated based on the starting PhIO. 2 mol of PhIO were considered for the formation of 1 mol of ketone or aldehyde. 1-heptanol = 1-ol, 2-heptanol = 2-ol, 3-heptanol = 3-ol, 4-heptanol = 4-ol, 2-heptanone = 2-one, 3-heptanone = 3-one, and 4-heptanone = 4-one.

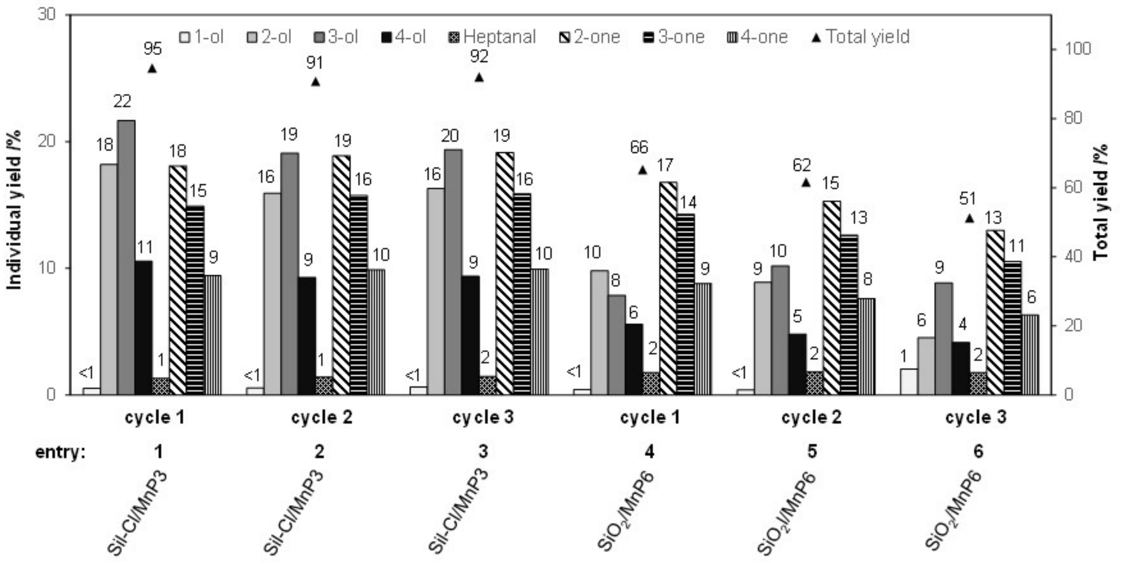

Figure S19. First cycle (cycle 1), second (cycle 2), and third (cycle 3) cycles of n-heptane oxidation reactions by PhIO catalyzed by the supported materials **Sil-Cl/MnP3** and **SiO_2/MnP6**. After completion of cycle 1, the catalysts were recovery and reused for twice more consecutively (cycles 2 and 3). The reaction conditions were identical to those of Figure 5, except that n-heptane replaced cyclohexane and the MnP/PhIO/n-heptane molar ratio was of 1:10:5000. Yields calculated based on the starting PhIO. 2 mol of PhIO were considered for the formation of 1 mol of ketone or aldehyde. 1-heptanol = 1-ol, 2-heptanol = 2-ol, 3-heptanol = 3-ol, 4-heptanol = 4-ol, 2-heptanone = 2-one, 3-heptanone = 3-one, and 4-heptanone = 4-one.

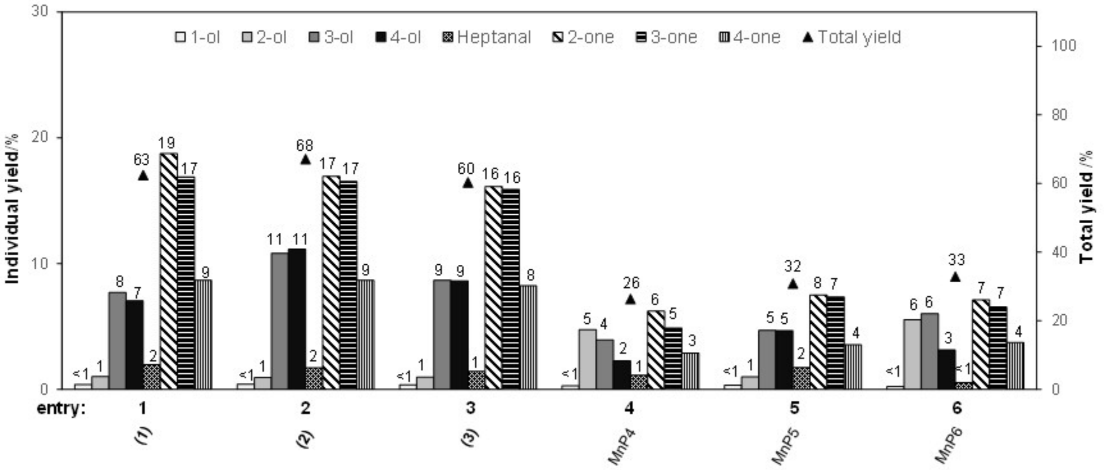

Figure S20. n-Heptane oxidation by PhIO catalyzed by non-immobilized **MnPY** and **MnPY** under homogeneous conditions. The conditions were identical to those of Figure 5. Yields calculated based on the starting PhIO. 2 mol of PhIO were considered for the formation of 1 mol of ketone or aldehyde. 1-heptanol = 1-ol, 2-heptanol = 2-ol, 3-heptanol = 3-ol, 4-heptanol = 4-ol, 2-heptanone = 2-one, 3-heptanone = 3-one, and 4-heptanone = 4-one.

Table S4. Chemoselectivity and Regioselectivity of nheptane PhIO-oxidations catalyzed by recycled **SilCl/MnPY** and **SiO_2/MnPY** materials (cycle 2). Catalysts recovered from a first reaction run (Table 2 in the main article). The reaction conditions are indicated in the legend of Figure 7. Yields calculated based on the starting PhIO. 2 mol of PhIO were considered for the formation of 1 mol of ketone or aldehyde.

Entry	Catalyst	Total yield /%		Chemoselect.[c] /%	Regioselectivity[g] /%		
		C-OH[a]	C=O[b]		ω-1[d]	ω-2[e]	ω-3[f]
1	**Sil-Cl/MnP1**	43	39	53	34	31	34
2	**Sil-Cl/MnP2**	44	40	52	33	32	34
3	**Sil-Cl/MnP3**	45	46	49	32	32	35
4	**SiO_2/MnP4**	30	34	46	37	29	31
5	**SiO_2/MnP5**	19	33	37	35	30	33
6	**SiO_2/MnP6**	24	37	39	33	31	34

[a] C-OH: alcohols. [b] C=O: ketones + aldehyde. [c] Chemoselectivity = (C-OH)/[C-OH + C=O). [d] ω-1: sum of 2-ol and 2-one, [e] ω-2: sum of 3-ol and 3-one, [f] ω-3: sum of 4-ol and 4-one. [g] Normalized regioselectivity (ω-1) = 100 x [(2-ol + 2-one)/2]/{[(1-ol+1-heptanal)/3] + [(2-ol + 2-one)/2] + [(3-ol + 3-one)/2] + (4-ol + 4-one)}, normalized regioselectivity (ω-2) and normalized regioselectivity (ω-3) were calculated analogously.

Table S5. Chemoselectivity and Regioselectivity of nheptane PhIO-oxidations catalyzed by recycled **SilCl/MnPY** and **SiO$_2$/MnPY** materials (cycle 3). Catalysts recovered from a second reaction run (Table S4 above). The reaction conditions are indicated in the legend of Figure 7. Yields calculated based on the starting PhIO. 2 mol of PhIO were considered for the formation of 1 mol of ketone or aldehyde.

Entry	Catalyst	Total yield /%		Chemoselect.[c] /%	Regioselectivity[g] /%		
		C-OH[a]	C=O[b]		ω-1[d]	ω-2[e]	ω-3[f]
1	**Sil-Cl/MnP1**	43	42	51	34	31	33
2	**Sil-Cl/MnP2**	37	36	51	33	32	33
3	**Sil-Cl/MnP3**	46	46	50	32	32	35
4	**SiO$_2$/MnP4**	30	38	44	37	29	31
5	**SiO$_2$/MnP5**	18	30	38	35	30	33
6	**SiO$_2$/MnP6**	20	32	38	29	32	35

[a] C-OH: alcohols. [b] C=O: ketones + aldehyde. [c] Chemoselectivity = (C-OH)/[C-OH + C=O). [d] ω-1: sum of 2-ol and 2-one, [e] ω-2: sum of 3-ol and 3-one, [f] ω-3: sum of 4-ol and 4-one. [g] Normalized regioselectivity (ω-1) = 100 x [(2-ol + 2-one)/2]/{[(1-ol+1-heptanal)/3] + [(2-ol + 2-one)/2] + [(3-ol + 3-one)/2] + (4-ol + 4-one)}, normalized regioselectivity (ω-2) and normalized regioselectivity (ω-3) were calculated analogously.

S13. Reactions of adamantane oxidation

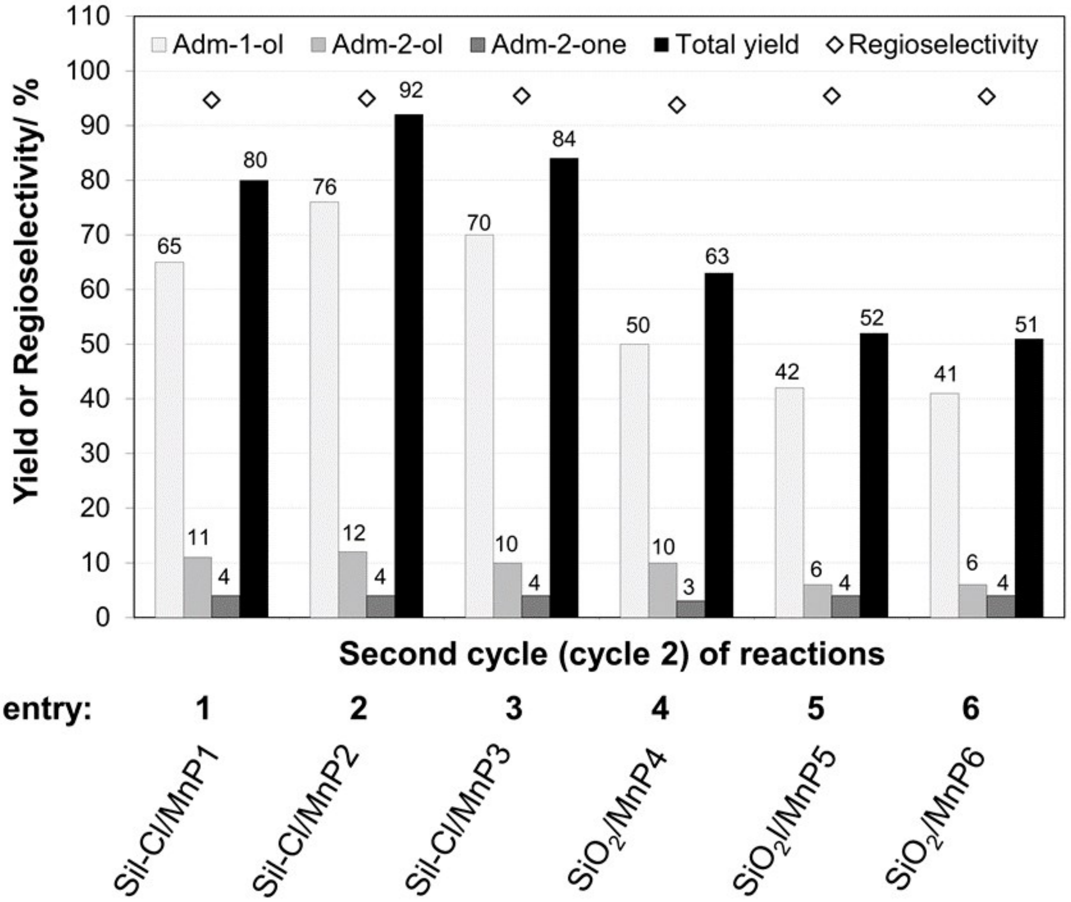

Figure S21. Second cycle (cycle 2) of adamantane oxidation reactions by PhIO catalyzed by the supported materials **Sil-Cl/MnPY** and **SiO$_2$/MnPY** after completion of cycle 1 (Figure 8) and catalyst recovery. The reaction conditions were the same as those described in Figure 8. 1-adamantanol = Adm-1-ol, 2-adamantanol = Adm-2-ol, total yield = Adm-1-ol + And-2-ol + Adm-2-one. Normalized regioselectivity = 100 x (Adm-1-ol)/[(Adm-1-ol) + (Adm-2-ol)/3 + (Adm-2-one)/3].

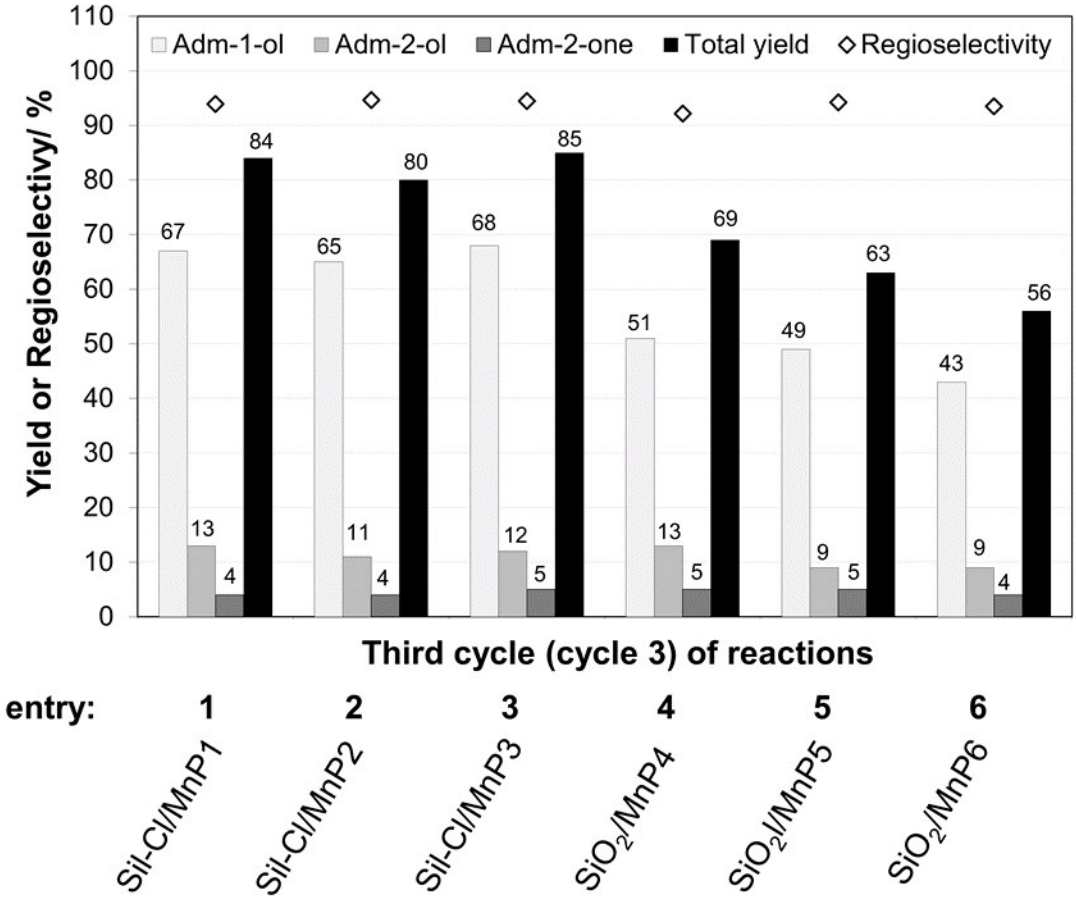

Figure S22. Third cycle (cycle 3) of adamantane oxidation reactions by PhIO catalyzed by the supported materials **Sil-Cl/MnPY** and **SiO$_2$/MnPY** after completion of cycle 2 (Fig. S21) and catalyst recovery. The reaction conditions were the same as those described in the Figure 8. Adm-1-adamantanol = Adm-1-ol, 2-adamantanol = Adm-2-ol, total yield = Adm-1-ol + Adm-2-ol + Adm-2-one. Normalized regioselectivity = 100 x (Adm-1-ol)/[(Adm-1-ol) + (Adm-2-ol)/3 + (Adm-2-one)/3].

References

1 J.S. Rebouças, M.E.M.D. Carvalho, Y.M. Idemori, *J. Porphyr. Phthalocyanines*, 2002, **6**, 50.

2 D.B.G. Williams, M. Lawton, *J. Org. Chem.,* 2010, **75**, 8351.

3 P. Worthington, P. Hambright, R.F.X. Williams, J. Reid, C. Burnham, A. Shamim, J. Turay, D.M. Bell, R. Kirkland, R.G. Little, N. Datta-Gupta, U. Eisner, *J. Inorg. Biochem.,* 1980, **12**, 281.

4 H. Saltzman, J.G. Sharefkin, *Org. Synth.*, 1963, **43**, 60.

5 V.L.S. Augusto Filha, O.G. da Silva, J.R. da Costa, A.F. Wanderley, M.G. da Fonseca, L.N.H. Arakaki, *J. Therm. Anal. Calorim.*, 2007, **87**, 621.

6 F. Wang, Z. Zhang, J. Yang, L. Wang, Y. Lin, Y. Wei, *Fuel, 2013,* **107**, 394.

7 P. Zhang, J. Chen, L. Jia, *J. Chromatogr. A*, 2011, **1218**, 3459.

8 Y. Wu, Z. Li, C. Xia, *Ind. Eng. Chem. Res.,* 2016, **55**, 1859.

9 C.V. Santilli, N.L.D. Filho, S.H. Pulcinelli, J.C. Moreira, Y. Gushikem, *J. Mater. Sci. Lett.*, 1996, **15**, 1450.

10 N.L.D. Filho, Y. Gushikem, E. Rodrigues, J.C. Moreira, W.L. Polito, *J. Chem. Soc. Dalt. Trans.,* 1994, **141**, 1493.

11 Q. Zhu, S. Maeno, R. Nishimoto, T. Miyamoto, M. Fukushima, *J. Mol. Catal. A Chem.,* 2014, **385**, 31.

12 M.S. Saeedi, S. Tangestaninejad, M. Moghadam, V. Mirkhani, I. Mohammadpoor-Baltork, A.R. Khosropour, *Polyhedron,* 2013, **49**, 158.

13 M. Moghadam, S. Tangestaninejad, M.H. Habibi, V. Mirkhani, *J. Mol. Catal. A Chem.*, 2004, **217,** 9.

14 M. Moghadam, S. Tangestaninejad, V. Mirkhani, I. Mohammadpoor-Baltork, A.A. Abbasi-Larki, *Appl. Catal. A Gen.*, 2008, **349**, 177.

15 M. Moghadam, S. Tangestaninejad, V. Mirkhani, I. Mohammadpoor-baltork, N. Sirjanian, S. Parand, *Bioorganic Med. Chem.,* 2009, **17**, 3394.

16 P. Battioni, J.P. Lallier, L. Barloy, D. Mansuy, *J. Chem. Soc., Chem. Commun.,* 1989, 1149.

17 A.M. Machado, F. Wypych, S.M. Drechsel, S. Nakagaki, *J. Colloid Interface Sci.,* 2002, **254**, 158.

18 G.M. Ucoski, V.H.A. Pinto, G. DeFreitas-Silva, J.S. Rebouças, I. Mazzaro, F.S. Nunes, S. Nakagaki, *ChemistrySelect*, 2017, **2**, 3703.

19 P.R. Cooke, J.R.L. Smith, *J. Chem. Soc. Perkin Trans. 1,* 1994, **14**, 1913.

20 F.S. Vinhado, C.M.C. Prado-manso, H.C. Sacco, Y. Iamamoto, *J. Mol. Catal. A Chem.*, 2001, **174** , 279.

21 L. Barloy, P. Battioni, D. Mansuy, *J. Chem. Soc. Chem. Commun.* 1990, 1365.

22 G.M. Ucoski, F.S. Nunes, G. Defreitas-Silva, Y.M. Idemori, S. Nakagaki, *Appl. Catal. A Gen.,* 2013, **459,** 121.

23 V.H.A. Pinto, D. CarvalhoDa-Silva, J.L.M.S. Santos, T. Weitner, M.G. Fonseca M.I. Yoshida, Y.M. Idemori, I. Batinić-Haberle, J.S. Rebouças, *J. Pharm. Biomed. Anal.*, 2013, **73**, 29.

24 G. de F. Silva, D.C. da Silva, A.S. Guimarães, E. do Nascimento, J.S. Rebouças, M.P. de Araujo, M.E.M.D. de Carvalho, Y.M. Idemori, *J. Mol. Catal. A Chem.,* 2007*,* **266**, 274.

25 A. Harriman, G. Porte, *J. Chem. Soc. Faraday Trans*. *2*, 1979, **75**, 1532.

26 I. Batinić-Haberle, L. Benov, I. Spasojević, I. Fridovich, *J. Biol. Chem.* 1998, **273**, 24521.

27 I. Batinić-Haberle, I. Spasojevic, P. Hambright, L. Benov, A.L. Crumbliss, I. Fridovich, *Inorg. Chem.*, 1999, **38**, 4011.

28 I. Batinić-Haberle, I. Spasojević, R.D. Stevens, P. Hambright, I. Fridovich, *J. Chem. Soc. Dalt. Trans.,* 2002, **13**, 2689.

29 J.S. Reboucas, I. Spasojević, I. Batinić-Haberle, *J. Pharm. Biomed. Anal.*, 2008, **48**, 1046.

30 J.S. Reboucas, I. Kos, Z. Vujaskovic, I. Batinić-Haberle. *J. Pharm. Biomed. Anal*., 2009, **50**, 1088.

31 G.A.M. Safar, Y.M. Idemori, D. CarvalhoDa-Silva, J.S. Rebouças, M.S.C. Mazzoni, A. Righi, *Nanotechnology,* 2012, 23 (2012) 275504.

32 A.N. de Sousa, M.E.M.D. de Carvalho, Y.M. Idemori, *J. Mol. Catal. A Chem.* 2001, **169**, 1.

33 V.H.A. Pinto, J.S. Rebouças, G.M. Ucoski, E.H. Faria, B.F. Ferreira, R.A.S.S. Gil, S. Nakagaki, *Appl. Catal. A Gen.,* 526 (2016) 9–20.

34 P. Battioni, J.P. Lallier, L. Barloy, D. Mansuy, *J. Chem. Soc., Chem. Commun.,* 1989, **01**, 1149.

35 A.M. Machado, F. Wypych, S.M. Drechsel, S. Nakagaki, *J. Colloid Interface Sci.,* 2002, **254**, 158.

36 M.A. Schiavon, Y. Iamamoto, O.R. Nascimento, M.D.D. Assis, *J. Mol. Catal. A Chem.*, 2001, **174**, 213.

37 G.S. Machado, O.J. de Lima, K.J. Ciuffi, F. Wypych, S. Nakagaki, *Catal. Sci. Technol.*, 2013, **3**, 1094.

38 J.R.L. Smith, Y. Iamamoto, F.S. Vinhado, *J. Mol. Catal. A Chem.,* 2006*,* **252** 23.

39 J.P. Collman, A. S. Chien, T.A. Eberspacher, J.I. Brauman, *J. Am. Chem. Soc.,* 2000, **122***,* 11098.

40 H. J. Lucas, E. R. Kennedy, *Org. Syntheses*, 1942, **22**, 72.

41 B. Meunier, *Chem. Rev.* 1992, **92**, 1411.

42 G.R. Friedermann, M. Halma, K.A.D. de F. Castro, F.L. Benedito, F.G. Doro, S.M. Drechsel, A.S. Mangrich, M. das D. Assis, S. Nakagaki, *Appl. Catal. A Gen.* 2006, **308**, 172.

43 D. Dolphin, T. Wijesekera, in *Metalloporphyrins in Catalytic Oxidations*, ed. R.A. Sheldon, Marcel Dekker, New York, 1994, 7, 193–293.